Numerical analysis of hydraulic jumps using OpenFOAM

Arnau Bayon-Barrachina, Petra Amparo Lopez-Jimenez

Deptartment of Hydraulic and Environmental Engineering – Universitat Politècnica de València,
Cami de Vera, s/n, 46022, Valencia (Spain),
Email: arbabar@iiama.upv.es, Tel: (+34) 96 387 9894.

Abstract

The present paper deals with the hydraulic jump study, characterization and numerical modeling. Hydraulic jumps constitute a common phenomenon in hydraulics of open channels that increases the shear stress on streambeds, so promoting their erosion. A three-dimensional computational fluid dynamics (CFD) model is proposed to analyze hydraulic jumps in horizontal smooth rectangular prismatic open air channels (i.e. the so-called classical hydraulic jump). Turbulence is modeled using three widely used RANS models, namely: Standard $k-\varepsilon$, RNG $k-\varepsilon$ and SST $k-\omega$. The coexistence of two-fluids and the definition of an interface between them are treated using a volume method in Cartesian grids of several element sizes. An innovative way to deal with the outlet boundary condition that allows reducing the size of the simulated domain is presented. A case study is conducted for validation purposes ($Fr_1 \sim 6.10$, $Re_1 \sim 3.5 \cdot 10^5$): several variables of interest are computed (sequent depths, efficiency, roller length, free surface profile, etc.) and compared to previous studies, achieving accuracies above 98% in all cases. In the light of the results, the model can be applied to real-life cases of design of hydraulic structures.

Keywords: Hydraulic jump; Open channel; OpenFOAM; RANS;k-epsilon; k-omega.

Nomenclature

AAN	Artificial Neural Network
SPH	Smoothed Particle Hydrodynamics
CFD	Computational Fluid Dynamics

DNS	Direct Numerical Simulation
LES	Large Eddy Simulation
RANS	Reynolds-Averaged Navier-Stokes
RNG	Re-Normalization Group
SST	Shear Stress Transport
FVM	Finite Volume Method
VOF	Volume of fluid
u	freestream velocity
u_c	compression velocity
u_τ	shear velocity
p	Pressure
t	Time
q	inlet flow rate
x_i	Cartesian reference system component
f_b	body forces
ρ	fluid density
h	water depth
H	hydraulic head
ΔH	energy drop
η	hydraulic jump efficiency
Γ	dimensionless water depth
k	turbulent kinetic energy
ε	dissipation rate of turbulent kinetic energy
ω	specific dissipation rate of turbulent kinetic energy
μ	dynamic viscosity
μ_t	turbulent eddy dynamic viscosity
ν	kinematic viscosity
ν_t	turbulent eddy kinematic viscosity
P_k	production of turbulent kinetic energy
P_b	effect of buoyancy
Y_M	effect of dilatation
S_k , S_ε	modulus of mean rate-of-strain tensor
$C_{1\varepsilon}$, $C_{2\varepsilon}$, $C_{3\varepsilon}$	model parameters

σ_k, σ_ε	model parameters
g	acceleration of gravity
Δx	mesh element size
C_μ	model parameter
α	water fraction in mesh element
Fr	Froude number
Re	water-height-based Reynolds number
Ma	Mach number
Cr	Courant number
w	channel width
x_1	position of hydraulic jump toe
x_2	position of roller end
x_3	position of hydraulic jump end
X	dimensionless longitudinal coordinate
L_j	length of hydraulic jump
L_r	length of roller
ξ_i	generic flow property of fluid "i"
Y	ratio of sequent depths
y^+	dimensionless wall distance
u^+	dimensionless velocity
E_i	error in variable i results
R^2	coefficient of determination
*	superindex relative to classical hydraulic jump
$_1$	subindex relative to supercritical flow
$_2$	subindex relative to subcritical flow

Introduction

Hydraulic jumps are the most used method to dissipate energy in hydraulic structures and occur in water flows suddenly changing of regime from supercritical to subcritical. This virulent phenomenon is characterized by large pressure and velocity fluctuations, air entrainment and turbulent dissipation processes. It can therefore trigger erosion processes or scour on hydraulic structures of calamitous consequences. By definition, hydraulic jumps occur in gravity-driven flows when the Froude number (ratio of inertia to gravitational forces) drops below unity. The Froude number is a dimensionless number of Fluid Mechanics that, in horizontal channels at a given section i, can be computed as Eq. 1 indicates:

$$Fr_i = \frac{u_i}{\sqrt{g h_i}} \tag{1}$$

Where u_i is flow freestream velocity, g, acceleration of gravity, and h_i, water depth. Despite the fact that the nature of hydraulic jumps is essentially chaotic, within a certain range of approaching Froude numbers (Fr_1), this phenomenon can become stable to a certain extent. According to Hager (1992) stabilized hydraulic jumps occur when $Fr_1 \in [4.5, 9.0]$. Lower values produce transition jumps, characterized by low efficiencies and the formation of long waves of irregular period, whereas higher Froude numbers produce choppy jumps, which are unstable and prone to flow detachment and wave and spray formation. For this reason, most of stilling basin design guidelines, such as that of the U.S. Bureau of Reclamation (Peterka, 1984), recommend aiming at Froude number values that produce stabilized hydraulic jumps.

Characterizing and analyzing this phenomenon is of paramount importance from both the technical and the environmental point of view. Hager (1992) and Chanson (2013) performed extensive reviews on the attempts to study this phenomenon throughout history. Some of these works focused in a theoretical comprehension of the characteristic features of the classical hydraulic jump. The so-called classical hydraulic jump is defined by Hager (1992) as the hydraulic jump that occurs in smooth horizontal prismatic rectangular channels. Resch and Leutheusser (1972) performed a thorough study on air entrapment and energy dissipation processes depending on the inlet flow characteristics. Gualtieri and Chanson (2007) extended this analysis to a wider range of inlet flow conditions.

Most of the studies performed up until today focused on the analysis of easily-measurable external macroscopic variables using an experimental approach. This can partially be explained by the difficulty of

measuring certain variables using non-intrusive acoustic and optical methods in highly aerated flows (Murzyn *et al.*, 2005). However, since the 1970s, coinciding with the emergence of computational fluid dynamics (CFD), more and more studies on the hydraulic jump are conducted by means of numerical methods. In this regard, computational techniques brought a brand new approach to water engineering modeling. E.g., some hard-to-model phenomena, such as heat transfer (Thomas *et al.*, 1990) or coupled biological processes (Muttil and Chau, 2006), could be for the first time implemented thanks to numerical methods. This implied a whole paradigm shift and so the literature on this topic is vast: e.g. Ma *et al.* (2011), among others, modeled hydraulic jumps using different CFD techniques. Caisley *et al.* (1999) managed to reproduce accurately a hydraulic jump in a canoe chute using FLOW-3D. Also Bombardelli *et al.* (2011) used this commercial software to successfully model a stepped spillway following a similar approach of that proposed here. Other approaches different from CFD have also been used in all kind of water engineering applications. E.g. De Padova *et al.* (2013) successfully reproduced a hydraulic jump using techniques of Smoothed Particle Hydrodynamics (SPH).

However, as Murzyn and Chanson (2009a) state, mathematical models still have problems to reproduce the physics of certain hydraulic phenomena, although they can contribute to their better comprehension. As Romagnoli *et al.* (2009) remark, an entire comprehension of the hydraulic jump internal flow features and turbulence structures has not been achieved so far. For Murzyn and Chanson (2009a), the main features of hydraulic jumps that have not been fully understood are the following: fluid mixing, bubble break-up and coalescence, free surface turbulent interactions and wave formation and breaking processes.

Other authors used a CFD approach to analyze hydraulic jumps in terms of shear stresses, potential erosion on stream boundaries and other more practical applications (Chanson, 2000). Liu and Garcia (2008) published a model combining the CFD code OpenFOAM and the Exner Equation to model erosion and sedimentation processes in hydraulic structures using mesh deformation.

Nevertheless, despite the increasing number of publications in this area, in the numerical modeling of hydraulic structures and water engineering applications, deterministic models (e.g. CFD) are overwhelmed in number by their statistical counterparts, also known as “black box” models (Chau *et al.*, 2005). Thus, several authors used artificial neural networks (AAN) to successfully predict the scour occurred at hydraulic structures, such as bridge piers (Toth and Brandimarte, 2011) or culvert outlets (Liriano and Day, 2001). Taormina *et al.* (2012) and Cheng *et al.* (2005) used AAN to successfully predict aquifer discharge processes. Farhoudi *et al.* (2010) used fuzzy logic methods to analyze the scour downstream of stilling basins. Other authors used one-dimensional and two-dimensional approaches to

reproduce the flow in similar geometries (Dewals *et al.*, 2004). However, in hydraulic engineering, flows are generally strongly three-dimensional (Ahmed and Rajaratnam, 1997). Therefore, the use of a fully three-dimensional deterministic model, such as here proposed, allows its application to a wider range of cases. Comparisons among different numerical methods to model hydrological and hydraulic phenomena can be found in the literature (Chen and Chau, 2006; Wu *et al.*, 2009).

The main goal of this work is to propose a fully three-dimensional CFD-based method to model classical hydraulic jumps using the open-source platform OpenFOAM. The use of freely-available open source codes allows a continuous community-based improvement of the model and avoids having to pay for costly software licenses. In this sense, other models can be found, also reproducing hydraulic jumps using OpenFOAM (Romagnoli *et al.*, 2009; Witt *et al.*, 2013). However, different outlet boundary conditions are herein presented. This change constitutes an asset as it allows bringing the model boundaries closer to the hydraulic jump, which involves a significant saving of computational resources.

A case study is also conducted, where several variables of interest, such as hydraulic jump efficiency or roller length, are computed and compared to previous analytical and experimental studies. The sensitivity of the model to certain parameters, such as mesh element size, turbulence model used or boundary conditions, is assessed.

As discussed in further sections, given the result accuracy achieved, this model is fully applicable to more complex geometries where hydraulic jumps have to be investigated, such as dam spillways, stilling basins, river rapids, etc.

Methods

Geometry and mesh

In this model of the hydraulic jump, the geometry to discretize is rather simple: the domain consists of a prismatic rectangular channel. For this discretization, two big categories of approaches are normally used, namely: unstructured and structured meshing.

Unstructured meshes are generally better suited for a selective refinement, so preventing the over-refinement of regions where no large gradients of property are expected (Kim and Boysan, 1999).

Besides, this kind of meshes fit better into complex geometries, show less closure issues and their arbitrary topology makes automatizing the meshing process easier (Biswas and Strawn, 1998). Nevertheles, none of these advantages applies to the case under study, as the geometry is extremely simple and no mesh refinement is required.

Some authors state that mesh non-orthogonality does not affect results as long as the skewness of its elements is kept low enough (Huang and Prosperetti, 1994). Nevertheless, structured meshes tend to be more accurate than their unstructured counterparts caeteris paribus (Biswas and Strawn, 1998). Besides, structured meshing algorithms are generally more straight forward to implement and faster to execute. According to Keyes *et al.* (2000) structured meshing algorithms present a more regular access to memory, which significantly reduces its latency. Also, as discussed below, in multiphase flows, topologically orthogonal meshes with their axis aligned with the fluid interface tend to show less numerical problems. For all these reasons, a static structured rectangular hexahedral mesh is considered the best choice.

In some cases, meshes can be slightly refined in the vicinity of solid boundaries for accurately resolving the flow features in boundary layers, where larger property gradients occur. This may result in the formation of highly skewed elements, although this is not a real issue as long as orthogonality between the mesh axes and solid boundaries is ensured (Hirsch, 2007). However, in this case, experience demonstrates that the mesh element size necessary to capture the freestream flow features is not smaller than that necessary to resolve the boundary layer features. As a consequence, cubic mesh elements of uniform size Δx are used throughout the entire domain (see Fig. 1). The optimum mesh element size is highly case specific so, it is determined by means of a mesh sensitivity analysis.

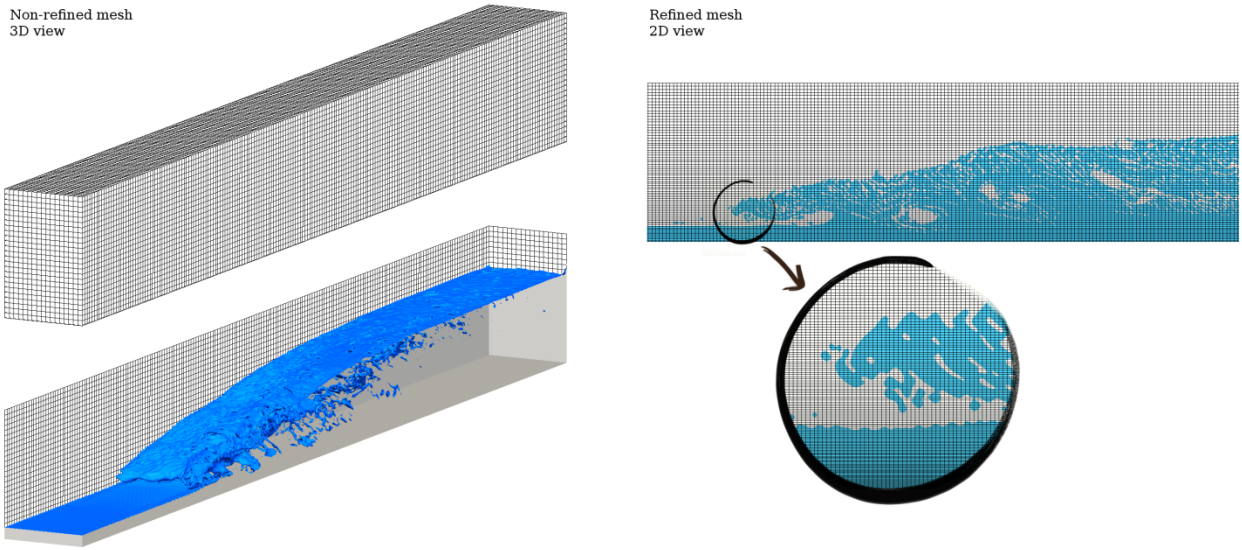

Figure 1. Example of a mesh used in the model with zoom on the jump toe region.

Numerical model

Water level of open channel flows can be obtained by shallow wave approaches. However, they are not sufficient when modeling complex geometries as only a water depth value is assigned to each point on the streambed. In cases where a full description of the flow characteristics is necessary, resolving the Navier-Stokes Equations becomes a must. Eq. 2 and 3 are the Navier-Stokes Equations for mass and momentum conservation in their incompressible form. Unfortunately, their complete analytical resolution has not been achieved so far, so numerical models are necessary to approximate a solution to every problem involving fluid motion.

$$\nabla \bar{u} = 0 \tag{2}$$

$$\frac{\partial \bar{u}}{\partial t} + \bar{u} \cdot \nabla \bar{u} = -\frac{1}{\rho}\nabla p + \upsilon \nabla^2 \bar{u} + \bar{f_b} \tag{3}$$

Where u is velocity, p, pressure, t, time, ρ, density, υ, kinematic viscosity, and f_b, body forces (gravity and surface tension). The flow is assumed to be incompressible in order to save computational resources and so density varying terms have been cancelled out. This assumption can be done as Mach numbers (ratio of the flow velocity to the sound velocity) are below the commonly accepted threshold of $Ma < 0.3$ (Young *et al.*, 2010).

A wealth of algorithms has been developed to approximate numerically the Navier-Stokes Equations during the last decades. Nevertheless, none of them constitutes a perfect solution as their performance is highly case specific. Indeed, this is a topic extensively discussed in the literature (Barton, 1998; Jang *et al.*, 1986). It is important to remark that the algorithm performances are generally assessed in terms of computation requirements and stability as, eventually, all algorithms should converge to a similar solution. The most widely used algorithm to execute stationary simulations and normally the default option in all CFD codes is the SIMPLE algorithm (Patankar and Spalding, 1972). Several improvements to its original implementation, such as SIMPLER or SIMPLEC, have been made since the model was developed. One of the most used variations is the PISO algorithm (Issa, 1985). However, problems may arise when dealing with multiphase flows where phase changes are abrupt or the density difference is large (Brennan, 2001). In order to overcome this issue, an algorithm was developed combining the best

features of SIMPLE and PISO; the so-called PIMPLE (OpenFOAM, 2011). This algorithm merges the outer-correction tools of SIMPLE with the inner-corrector loop of PISO in order to achieve a more robust and generalizable pressure-velocity coupling (Rodrigues *et al.*, 2011).

Hence, the PIMPLE algorithm is here used as a good compromise between computation requirements and stability. This algorithm is implemented in OpenFOAM, a freely available open source platform constituted by all sort of C++ applications and libraries to solve all kinds of continuum mechanics problems (Weller *et al.*, 1998). This code uses a tensorial approach and object-oriented programming techniques following the widely known Finite Volume Method (FVM), first used by McDonald (1971). An in-depth explanation of the algortihm implementation can be found in the PhD Thesis of Jasak (1996), Ubbink (1997) and Rusche (2002).

Water surface tracking

The coexistence and interaction of several fluids and the way that the interface among them is defined is of paramount importance in numerical modeling of multiphase flows. Complex algorithms must be developed to model this phenomenon, whose stability and accuracy have a strong influence on the model final results (Hyman, 1984). Surface tracking methods fall into two families of approaches, namely: the surface methods and the volume methods. On the one hand, surface methods explicitly define the free interface either using a Lagrangian approach, i.e. tracking a set of surface marker particles (Daly, 1969), or using an Eulerian approach, i.e. defining functions that determine the free surface position (Osher and Sethian, 1988). These methods present topology issues when dealing with highly deformed flows and breaking surfaces. For this reason, they are not considered appropriate to model hydraulic jumps.

On the other hand, volume methods adapt better to this kind of phenomena, but do not define a neat flow interface explicitly. Instead, a surface tracking method has to be implemented in the model. Some models use an Eulerian-Lagrangian approach (particles on fluid methods) combining an Eulerian flow resolution with particle tracking (Harlow and Welch, 1965). However, in three-dimensional models, the large number of necessary particles makes the computational cost of this approach unaffordable. For this reason, an entirely Eulerian approach is used in the present model. This kind of approaches proved to be more computationally efficient as they only have to deal with a single variable value per mesh element (Ubbink, 1997). This variable is an indicator property (α) expressing the proportion of one fluid or another that every mesh element contains. Its distribution throughout the domain is modeled by approximating an additional convection transport equation (Eq. 4). This implies considering both fluids,

A and B, as a single multiphase fluid, whose properties are treated as weighted averages according to the fraction occupied by one fluid or another in each mesh element (see Eq. 5). This results in a set of α values between 0 and 1 throughout the entire modeled domain but no clear water-air interface is defined a priori.

$$\frac{\partial \alpha}{\partial t} + \nabla \cdot (\bar{u}\ \alpha) = 0 \tag{4}$$

$$\xi = \xi_a \alpha + \xi_b (1 - \alpha) \tag{5}$$

Where α is fluid fraction, u, velocity, t, time, and ξ represents a flow generic property. As regards the method used to clean up the misty zones and so define a neat interface, a wealth of approaches has been developed during the last decades. The traditional line techniques, such as SLIC (Noh and Woodward, 1976), PLIC (Youngs, 1984) or FLAIR (Ashgriz and Poo, 1991), provided the first viable solutions to the surface definition issue in volume methods. However, they present problems of generalization to unstructured meshes. The donor-acceptor methods, such as the original implementation of the VOF (Hirt and Nichols, 1981), have been widely used in the past, but they are prone to show false interface deformation issues.

In the present model, an interface compression algorithm is implemented in order to overcome the aforementioned issues. This method adds an extra term in the left hand side of Eq. 4: $\nabla \cdot (\overline{u_c}\ \alpha[1 - \alpha])$, where $\overline{u_c}$ is a compression velocity with normal direction to the fluid interface. Multiplying $\overline{u_c}$ by $\alpha[1 - \alpha]$ ensures that it will only affect those regions where the flow fraction is close to 0.5 (Rusche, 2002).

Flow aeration

The aeration of a water flow modifies its volume, depth, density and compressibility (Carvalho, 2002), thus affecting the momentum transfer. It also reduces the scour risk by cavitation (Bung and Schlenkhoff, 2010) and the shear stresses on the channel boundaries (Chanson, 1994). Therefore, this is a phenomenon of paramount importance in highly aerated flows as hydraulic jumps, bores, breaking waves, etc. Unfortunately, surface tracking methods per se cannot reproduce phenomena smaller than the mesh element size, such as bubbles and droplets, or the entrapment of large amounts of air (Toge, 2012). To overcome this issue, additional air-entrainment models are implemented. In low-aerated flows, an Eulerian-Lagrangian approach is possible, where the Navier-Stokes Equations are resolved and air is treated as a set of discrete particles. With larger air fractions, this approach is no longer possible and an

entirely Eulerian method is necessary. Eulerian-Eulerian approaches yield better results than their Eulerian-Lagrangian counterparts in the latter case. Despite the fact that they require longer computation times, in entirely Eulerian approaches, buoyancy, drag and lift forces are taken into account. For this reason, in the case of the model proposed here, an Eulerian-Eulerian approach is implemented.

Turbulence

Turbulence features can either be resolved down to their lowest scales (Direct Numerical Simulation or DNS), if the mesh is accordingly fine, or modeled under a wealth of different approaches. Despite it has been reported the application of DNS models to multiphase flows (Borue *et al.*, 1995), in most cases turbulence features are partial or completely modeled in common engineering applications.

Large Eddy Simulation (LES) approaches are also feasible to model multiphase flows. Nevertheless, the most used technique is the Reynolds Averaged Navier-Stokes (RANS). In these models, the so-called Reynolds stresses are averaged to find a closure to the Navier-Stokes equations. To do so, additional transport equations are implemented in order to model the behavior of flow turbulence. Among the available models, the performance of three of the most used is here studied. The assessed models are the Standard $k-\varepsilon$ (Launder and Sharma, 1974), the RNG $k-\varepsilon$ (Yakhot *et al.*, 1992) and the SST $k-\omega$ (Menter, 1993). The Standard $k-\varepsilon$ model has been widely used in this kind of applications (López and Garcia, 2001). Its formulation is depicted in Eq. 6 and 7:

$$\frac{\partial}{\partial t}(\rho k)+\frac{\partial}{\partial x_i}(\rho k u_i)=\frac{\partial}{\partial x_j}\left[\left(\mu+\frac{\mu_t}{\sigma_k}\right)\frac{\partial k}{\partial x_j}\right]+P_k+P_b-\rho\varepsilon-Y_M+S_k \tag{6}$$

$$\frac{\partial}{\partial t}(\rho \varepsilon)+\frac{\partial}{\partial x_i}(\rho \varepsilon u_i)=\frac{\partial}{\partial x_j}\left[\left(\mu+\frac{\mu_t}{\sigma_\varepsilon}\right)\frac{\partial \varepsilon}{\partial x_j}\right]+C_{1\varepsilon}\frac{\varepsilon}{k}(P_k+C_{3\varepsilon}P_b)-C_{2\varepsilon}\rho\frac{\varepsilon^2}{k}+S_\varepsilon \tag{7}$$

Where k is turbulence kinetic energy, ε, dissipation rate of k, t, time, ρ, density, x_i, coordinate in the i axis, μ, dynamic viscosity, μ_t, turbulent dynamic viscosity, P_k, production of turbulent kinetic energy, P_b, buoyancy effect, Y_M, dilatation effect, and S_k and S_ε, modulus of mean rate-of-strain tensor. The rest of terms, (C_μ, $C_{1\varepsilon}$, $C_{2\varepsilon}$, $C_{3\varepsilon}$, σ_k, and σ_ε) are model parameters that, in the Standard $k-\varepsilon$ model, are 0.09, 1.44, 1.92, -0.33, 1.0, and 1.3, respectively.

The RNG $k-\varepsilon$ model formulation differs from that of the Standard $k-\varepsilon$, essentially, in the values of the aforementioned parameters. These changes seem to improve the model results to such an extent that, according to Bradshaw (1996), the RNG $k-\varepsilon$ is the most used model in hydraulic applications.

Several authors claim that $k-\varepsilon$ models are not suitable to model large adverse-pressure gradient flows (Menter, 1993; Wilcox, 1998). In order to overcome this issue, $k-\omega$ models were first introduced by Wilcox (1998). Their implementation is significantly different from that of $k-\varepsilon$, as the dissipation rate of turbulence kinetic energy (ε) is not modeled. Instead, a transport equation for its relative value ($\omega = \varepsilon/k$) is implemented. Among them, the SST $k-\omega$ (Menter, 1993) proved to perform better than the Standard and the BSL $k-\omega$.

The suitability of one model or another is highly case specific and differences from using one model or another are normally remarkable. Hence, in order to determine which model performs best at a reasonable computational cost, a sensitivity analysis is conducted. To do so, simulations are run using the three RANS models discussed above caeteris paribus.

Boundary conditions

The boundary conditions imposed to force the hydraulic jump to occur consist of a supercritical flow inlet, a subcritical flow outlet, smooth bottom and side walls and an upper open air patch (see Fig. 2). At the inlet, in order to fulfill the desired Froude number, a water depth (h_1) and a potential velocity profile are imposed using a Dirichlet boundary condition. The pressure value is defined as a null von Neumann boundary condition, so forcing a hydrostatic profile. As regards the inlet variables of the RANS model, i.e. k, ε and ω, they cannot be directly estimated from measurements. Instead, they are set to an arbitrary low value and a short initial stretch of channel is added in order for the flow to develop while approaching the hydraulic jump.

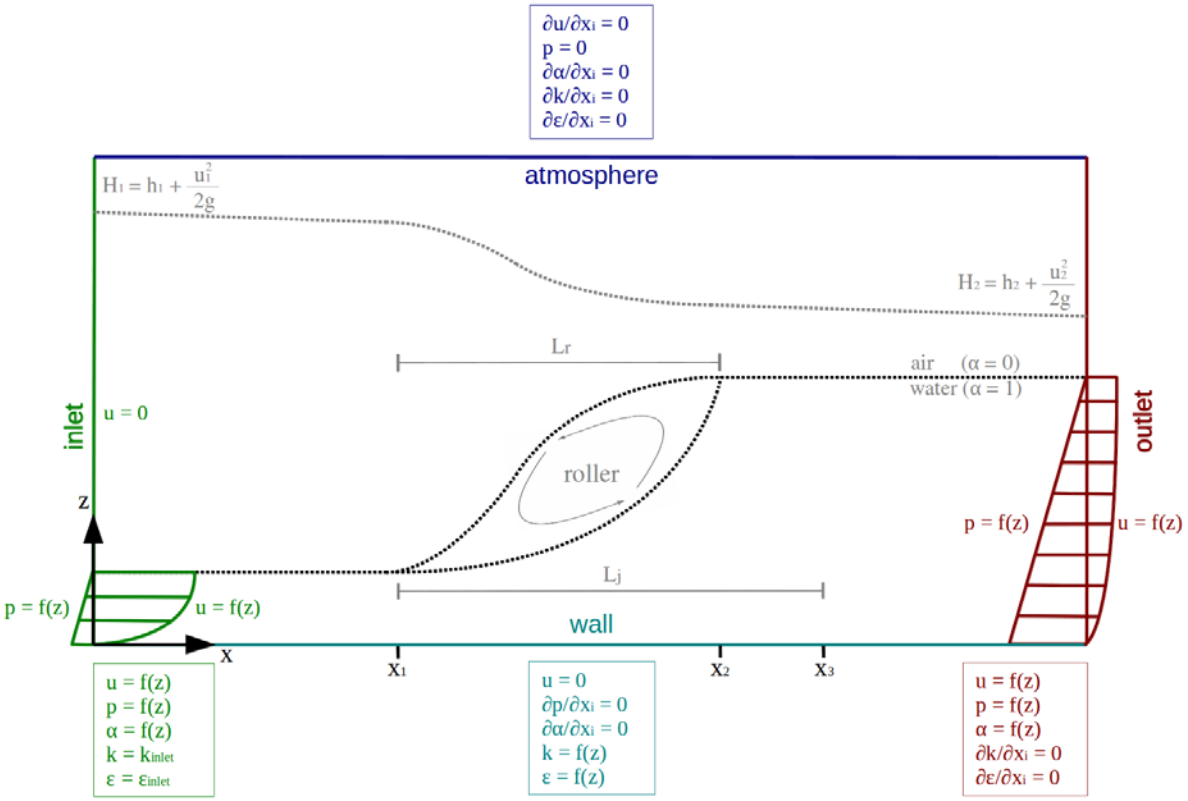

Figure 2. General scheme of a hydraulic jump and boundary conditions used in the model.

As regards the outlet, the subcritical water height that forces the hydraulic jump to occur within the simulated domain (h_2) has to be imposed. This variable has to be obtained by iteratively testing values until the resulting hydraulic jump remains stable within the domain. Normally, a subcritical water height and a hydrostatic profile should be imposed at the outlet by means of a Dirichlet water level boundary condition. This, combined with a null Von Neumann boundary condition for velocity, would allow the flow to leave the domain freely. However, the imposition of a subcritical outlet by means of this approach in OpenFOAM appears to cause stability issues.

Indeed, to the knowledge of the authors, all cases of hydraulic jump simulations using OpenFOAM reported in the literature, such as Romagnoli *et al.* (2009) or Witt *et al.* (2013), have had to bypass this issue. To do so, they added an additional stretch of channel with an obstacle on the streambed, such as a step, a gate or a ramp, followed by a conventional free outlet.

In the present model, this problem is overcome by imposing a velocity profile at the outlet and so letting the hydrostatic profile to develop, as it is done at the inlet boundary condition. Assuming mass conservation, this approach univocally produces a given water height. This avoids having to model the

aforementioned extra stretch of channel. As this implies bringing the boundary conditions closer to the phenomenon under study, comparative simulations are run in order to assess the model sensitivity to the boundary condition type.

A no-slip condition is imposed at the walls and roughness is not considered (Hager, 1992). An atmospheric boundary condition is imposed at the top of the channel to allow fluids to enter and leave the channel. This is achieved by imposing a null Von Neumann condition to all variables except for pressure, which is set to zero (atmospheric pressure). Fig. 2 summarizes the model boundary conditions and some of its most relevant variables to analyze.

Wall treatment

The way the boundary layer is treated is of paramount importance in fluid modeling. Von Karman (1930) established a universal law of the wall which defines the flow velocity profiles in the boundary layer. Velocity (u) and distance to wall (y) are respectively adimensionalized using the shear velocity (u_τ) and the viscosity (υ):

$$y^+ = y\frac{u_\tau}{\upsilon} \tag{8}$$

$$u^+ = \frac{u}{u_\tau} \tag{9}$$

The lowest y^+ regions, the so-called viscous sub-layer (Schlichting and Gersten, 2000), are characterized by large gradients of velocity and other properties and the predominance of viscous effects. In order to avoid having to resolve these regions, wall functions are often used in CFD models. These functions are imposed as boundary conditions on solid patches to avoid the use of excessively fine meshes, with the subsequent saving of computational resources. As a consequence, the model mesh has to be refined so that the y^+ coordinate of the center of all mesh elements in touch with solid walls be somewhere between the buffer and the logarithmic sub-layers ($y^+ \sim 30$). It is important not to over-refine meshes when using wall functions. If this happens, wall functions will be modeling the viscous sub-layer, whereas the model itself would be resolving the flow in this region. This controversy may cause that finer meshes yield less accurate results.

In terms of accuracy, the best choice would be using a low-Reynolds-number model with no wall function at all. However, this implies refining the mesh to such an extent that the computational cost may become unaffordable. There is vast literature on improvements to the original implementation of wall functions, such as Johnson and Launder (1982), but most of the solutions proposed have not been adopted by most of CFD codes. This is due to the fact that, despite these approaches are valid from a theoretical point of view, many of them may cause stability issues (Blocken *et al.*, 2007).

In this research, a high-Reynolds-number wall function for RANS models and smooth solid surfaces is implemented. The boundary layer in a case of these characteristics is likely to be slightly skewed (Taylor, 1959). Nevertheless, as the flow mainstream direction is completely longitudinal, a bi-dimensional wall function is used for the sake of simplicity.

Discretization schemes

As regards the discretization schemes used to make the CFD model partial differential equations numerically approximable, a good choice always must be a good compromise between accuracy and stability. In spatial discretization, upwind models are generally preferred to downwind approaches as the latter tend to show severe stability issues. Compared to central differencing schemes, upwind approaches are slower, but also less diffusive and so more accurate. The problem is that, when abrupt property gradients occur, the latter schemes may require limiters in order to prevent spurious oscillations (Blazek, 2005). Once limited, upwind schemes, such as Van Leer's (1982), are very appealing to discretize abruptly-varied properties. The only drawback is that, when limited, these schemes become first order accurate.

In the present model, the fluid fraction divergence terms (α) are discretized using a limited Van Leer approach due to its abruptly variable nature. In the case of the RANS model variables, divergence terms are discretized using an unlimited upwind approach as they are less prone to cause stability issues. The velocity divergence terms are discretized using a central differencing scheme in order to avoid possible instabilities as well as to reduce computation times. Also all gradient and interpolation terms of the model are discretized using this approach. Gaussian standard FVM is used to interpolate the variable values from cell centers to their faces. In order to save computational resources, as this mesh is strictly Cartesian, no orthogonality corrector is applied.

As regards the discretization of time derivatives, explicit schemes tend to be computationally lighter than their implicit homologues. However, they are also more unstable, especially, in simulations with skewed meshes (Blazek, 2005) or when solving RANS equations (Lafon and Yee, 1992). Therefore, implicit time discretization schemes are preferred in this model. This implies slightly longer computation times and eventual accuracy problems due to phenomena such as wave damping (Casulli and Cattani, 1994), but also higher stability. Hence, a first order accurate bounded implicit Euler scheme is used to discretize time derivative terms.

The time step length is variable throughout the simulation resolution process. Its value is automatically updated after every time step in order to ensure that the maximum Courant number never overcomes a threshold of $Cr < 0.75$, ensuring convergence and stability of simulations.

Postprocessing

The variables analyzed and compared to previous studies are discussed in the next lines. The reference values to which model results are compared are denoted by a super-index asterisk (*).

The sequent depth (Y), i.e. the ratio of subcritical to supercritical flow depth (h_1 and h_2, respectively), is a characteristic parameter of hydraulic jumps. According to Belanger (1841), it can be estimated as a function of the approaching Froude number using a series of simplifications of the Momentum Equation. Nevertheless, in channels of low aspect ratio (h_1/w), side walls can play an important role and this equation is no longer valid. In this regard, Murzyn and Chanson (2008) claim that scale effects can play an important role in channels of aspect ratio above 0.1. In order to overcome this issue, Hager and Bremen (1989) proposed the following approach introducing Blasius Equation to account for side wall friction effects, resulting:

$$Y^* = \frac{h_2}{h_1} = \frac{1}{2} \cdot \left[\sqrt{1 + 8 \cdot Fr_1^2} - 1\right] \cdot \left[1 - 0.7\,[\log Re_1]^{-2.5}\, e^{\frac{Fr_1}{8}}\right] \cdot \left[1 - 3.25\,\frac{h_1}{w}\, e^{\frac{Fr_1}{7}} (\log Re_1)^{-3}\right] \qquad (10)$$

Where h_1 is supercritical water depth, w, channel width, Fr_1, approaching Froude number, Re_1, supercritical height-based Reynolds number. Another relevant variable of hydraulic jumps is the roller length (L_r), i.e. the stretch right downstream of the jump toe where water recirculation occurs and most of the air entrainment occurs. Some authors, such as Murzyn and Chanson (2009b), define the roller length as the hydraulic jump region over which the water height increases monotonically. However, in this study

the stagnation point is used as a criterion to delimit the roller end. Hager (1992) proposes the following expression to estimate the roller length:

$$L_r^* = -12\,h_1 + 100 \cdot h_1 \cdot tanh\frac{Fr_1}{12.5} \quad (11)$$

The efficiency of hydraulic jumps is defined as the ratio of the energy drop to the upstream hydraulic head. These variables are obtained from Eq. 12 as a function of water height (h_i), flow velocity (u_i) and acceleration of gravity (g). Eq. 13 represents how hydraulic jump efficiency is computed. According to Hager and Sinniger (1985), in classical hydraulic jumps, the latter variable can be estimated as a function of the approaching Froude number using Eq. 14:

$$H_i = h_i + \frac{u_i^2}{2g} \quad (12)$$

$$\eta = \frac{\Delta H}{H_1} = \frac{H_1 - H_2}{H_1} \quad (13)$$

$$\eta^* = \left(1 - \frac{\sqrt{2}}{Fr_1}\right)^2 \quad (14)$$

Water surface levels are a variable of paramount importance in the design of hydraulic structures. Its accurate estimation is crucial for a proper stilling basin design that avoids bank bursts. In the present work, the average water surface levels are numerically computed and compared to the expression by Bakhmeteff and Matzke (1936):

$$\Gamma^*(x) = \tanh(1.5 \cdot X) \quad (15)$$

Where $\Gamma(x)$ is water level at x (h_i), non-dimensionalized following Eq. 16, where h_1 and h_2 are supercritical and subcritical water level, respectively. The variable X is the non-dimensional longitudinal coordinate (x), computed as a function of x_1 (hydraulic jump toe position) and x_2 (roller end position) as Eq. 17 indicates:

$$\Gamma(x) = \frac{h_i - h_2}{h_1 - h_2} \quad (16)$$

$$X = \frac{x - x_1}{x_2 - x_1} \quad (17)$$

The nature of hydraulic jumps is highly chaotic and unstable and so most of its characteristic variables show a quasi-periodic behavior (i.e. patterns can eventually be observed, but their characteristic period is not constant). For this reason, it is crucial to extend sufficiently the simulation time to avoid bias in the results. The authors observe that stability of the solution can be assumed when the residuals of all the variables drop below the 10^{-3} threshold and the water content of the whole modeled channel stays stable during at least $10s$.

Case study

A case particular study is conducted for validation purposes. The simulated case consists of a prismatic rectangular channel of dimensions $6.00m \times 0.50m \times 0.75m$ (length, width and height). The inlet flow is $q = 0.177m^3/s$ and the supercritical depth is $h_1 = 0.070m$. Hence, the inlet velocity is $u_1 = 5.057\, m/s$. The subcritical depth is obtained following the procedure discussed above in this section. The density and the kinematic viscosity are $\rho = 1000\, kg/m^3$ and $\upsilon = 10^{-6}\, m/s^2$.

The approaching Froude and Reynolds numbers are $Fr_1 = 6.125$ and $Re_1 = 3.54 \cdot 10^5$, respectively. A case of Fr_1 between 6 and 7 is considered optimum for model validation as it corresponds to the middle of the range of Fr_1 values recommended by the U.S. Bureau of Reclamation (Peterka, 1984). This approaching Froude number is assumed to be representative of the behavior of all stabilized hydraulic jumps, as described by Hager (1992).

As discussed above in this section, a mesh, turbulence and boundary condition model sensitivity analysis is conducted. Each of the turbulence models mentioned above (Standard $k-\varepsilon$, RNG $k-\varepsilon$ and SST $k-\omega$) are tested in four different sized meshes. The mesh element sizes assessed are $7.00mm$, $7.50mm$, $7.78mm$ and $8.75mm$, which means meshes of 6.511, 6.360, 4.737 and 3.467 million cells, respectively. In order to fulfill the wall treatment function hypothesis, it is checked in all cases that the y^+ coordinate mostly remains in the range of values between 20 and 70.

Results and discussion

Graphic analysis

A de visu analysis of the model results leads to the conclusion that a stabilized hydraulic jump is reached (see Fig. 3). All the characteristic features of this kind of jumps described by Hager (1992) can be observed, namely: compact and stable appearance, low wave generation, gradual bubble deaeration, vortex formation within the roller, no flow separation in the entering jet, etc. Fig. 3 shows how, downstream of the hydraulic jump, where bubble deaeration occurs, hydrostatic pressure and velocity profiles quickly reappear. Also the deaeration of large bubbles can be observed throughout the region where streamlines cut the water free surface. Downstream of that, despite waves and small bubbles do not disappear completely, the characteristics of developed flows can be observed again.

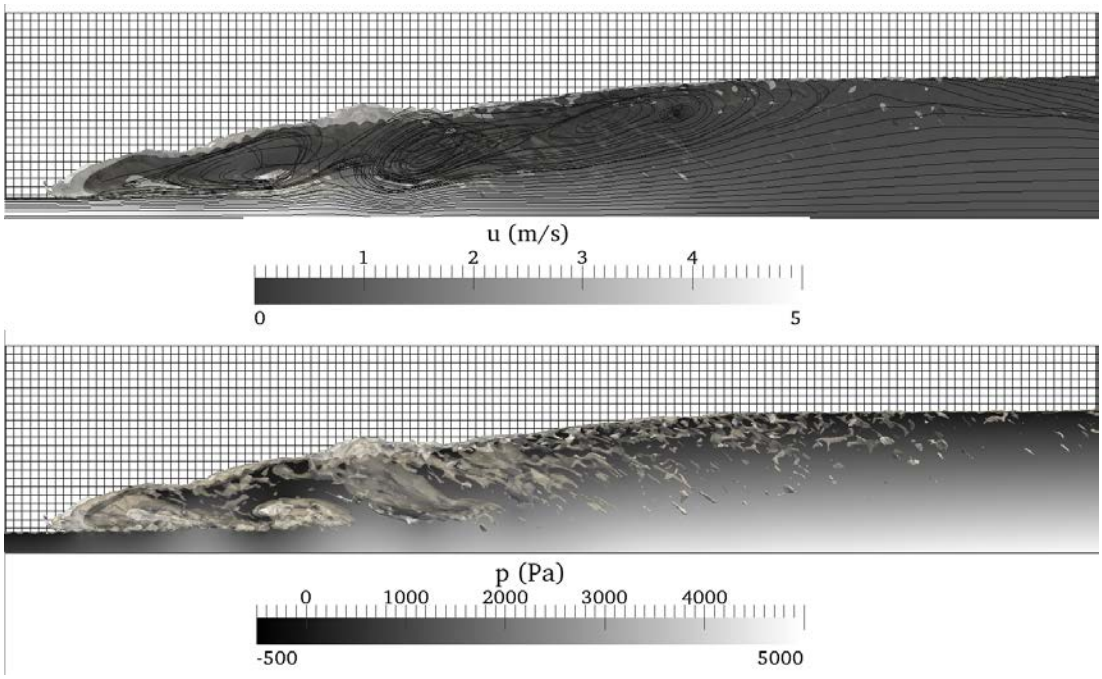

Figure 3. Instant representation of bubble formation and velocity and pressure fields.

Fig. 3 shows the wide span of bubble sizes occurred in the turbulent shear and the recirculation region of hydraulic jumps. Chanson (1994) found experimentally that the range of bubble sizes in hydraulic jumps can extend over several orders of magnitude. The average bubble size rapidly decreases longitudinally. This is due to the fact that large bubbles cannot stay long in the recirculation region as shear stresses break them up and buoyancy forces tend to expel them (Babb and Aus, 1981). Small bubbles are not deaerated so quickly. Indeed, they can be dragged by advection forces throughout long distances until buoyancy finally expels them.

Sensitivity analysis

As discussed above, a mesh, turbulence and boundary condition model sensitivity analysis is conducted in order to determine the best combination of them to achieve accurate results at an affordable computational cost.

As regards the outlet boundary condition used, Fig. 4 shows examples of hydraulic jumps simulated using both approaches. A closer comparison between them shows no significant effect on the model outcome accuracy. Although an instant comparison, such as that in Fig. 4, shows differences in water level profile and flow aeration, these differences completely disappear when results are averaged. No undesirable effects, such as wave formation, occur despite the new approach implies bringing the boundary conditions significantly closer to the phenomenon under study. The domain reduction achieves computation times up to 30% shorter in some cases.

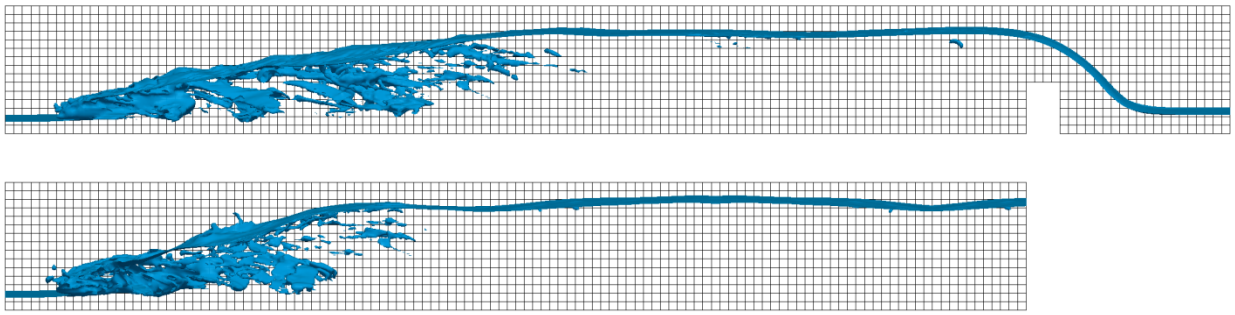

Figure 4. Instant comparison of hydraulic jumps simulated using two different outlet boundary conditions: the traditional approach (top) and a new approach (bottom).

The three tested turbulence models show small influence on the sequent depth (Y) estimations. The most accurate model is the RNG $k-\varepsilon$, followed by the SST $k-\omega$ and the Standard $k-\varepsilon$, although all errors are below 4%. The inflexion point in the accuracy of the all models can be clearly observed at a mesh size of $7.50mm$, thus being the RNG $k-\varepsilon$ model with $7.50mm$ size mesh the most accurate approach.

As regards the estimation of roller lengths, the SST $k-\omega$ model appears not to be able to capture accurately this variable. The Standard $k-\varepsilon$ model shows a reasonable accuracy (all errors are below 6%) and low sensitivity to mesh size, which is an asseet. However, RNG $k-\varepsilon$ is even more accurate and shows a perfect monotonically decreasing trend in errors, although the model is also highly sensitive to

mesh size variations. The RNG $k-\varepsilon$ model with $7.00mm$ size mesh appears to be the most accurate approach in the roller length prediction.

The prediction of the hydraulic jump efficiency achieves the highest accuracy values, being the error of all models below 2%. The Standard $k-\varepsilon$ with $7.00mm$ size mesh is the most accurate (0.1%) but, as it is observed in Fig. 5, the sensitivity of this variable to the model parameters is extremely low.

All further discussion on the results and model validation is exclusively conducted using the results of RNG $k-\varepsilon$ model with $7.00mm$ size mesh. The reason is because this approach achieved the most accurate results in the most sensitive variable (i.e. roller length) while being reasonably accurate in the prediction of the less sensitive variables.

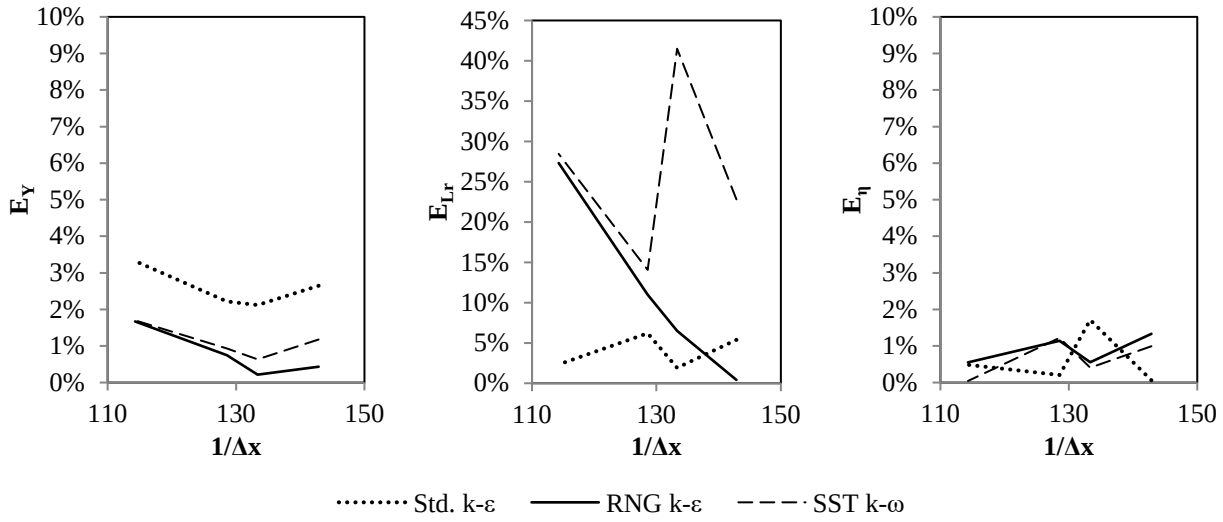

Figure 5. Mesh and turbulence model sensitivity analysis. Relative errors in the computation of sequent depths (Y), roller lengths (L_r) and hydraulic jump efficiency (η) with respect to bilbiography.

Quantitative analysis

The mean subcritical water depth obtained from the CFD model is $h_2 = 0.553m$, which leads to a mean ratio of sequent depths of $Y = 7.916$. Following Eq. 10, the reference value for this variable in classical hydraulic jumps is $Y^* = 7.951$. This means that the model yields a value approximately 0.4% lower than that obtained using the expression proposed by Hager and Bremen (1989).

Regarding the mean roller length, the model yields an mean value of $L_r = 2.320m$, being $L_r^* = 2.330m$ the value computed using Eq. 11. This implies an underestimation of only 0.4%. The accuracy in the prediction of this variable is crucial, as the largest shear stresses on the streambed generally occur within this stretch. In stilling basin design cases, this can be very helpful in order to determine the region of the structure that must be protected against scour.

Following Eq. 13, the mean efficiency of the hydraulic jump is $\eta = 58.2\%$. This agrees with the result obtained from Eq. 14 (Hager and Sinniger, 1985), which estimates an efficiency of 59.0%, with only a 1.3% error. The good agreement in the computation of these three variables compared to other works is depicted in Fig. 6.

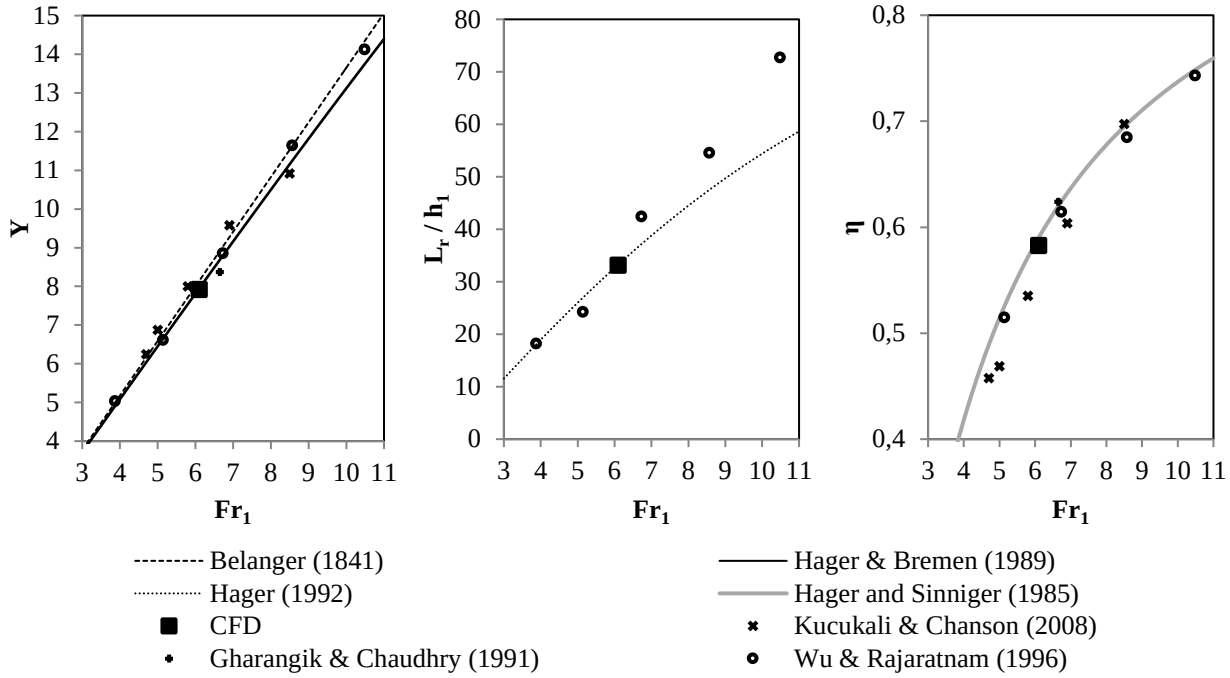

Figure 6. CFD model result comparison with analytical and experimental previous works. The analyzed variables are: sequent depth (Y), roller length (L_r) and hydraulic jump efficiency (η).

The comparison of water surfaces to previous studies (Bakhmeteff and Matzke, 1936) proves the consistency of the model presented herein. Fig. 7 shows the mean water levels computed using the three different turbulence models. The most accurate RANS model is the Standard $k-\varepsilon$ ($R^2 = 99.6\%$), followed by the RNG $k-\varepsilon$ ($R^2 = 99.2\%$) and the SST $k-\omega$ ($R^2 = 98.5\%$). It can be deduced from the above that turbulence models exert very little effect on the water free surface definition in average terms.

Nevertheless, an instant observation of the evolution of this variable shows that SST $k-\omega$ models produce a more unstable and bursting water surface with high bubble and spray production. Both $k-\varepsilon$ models produce smoother surfaces, being the Standard $k-\varepsilon$ also the model that yields a more uniform and less turbulent free surface.

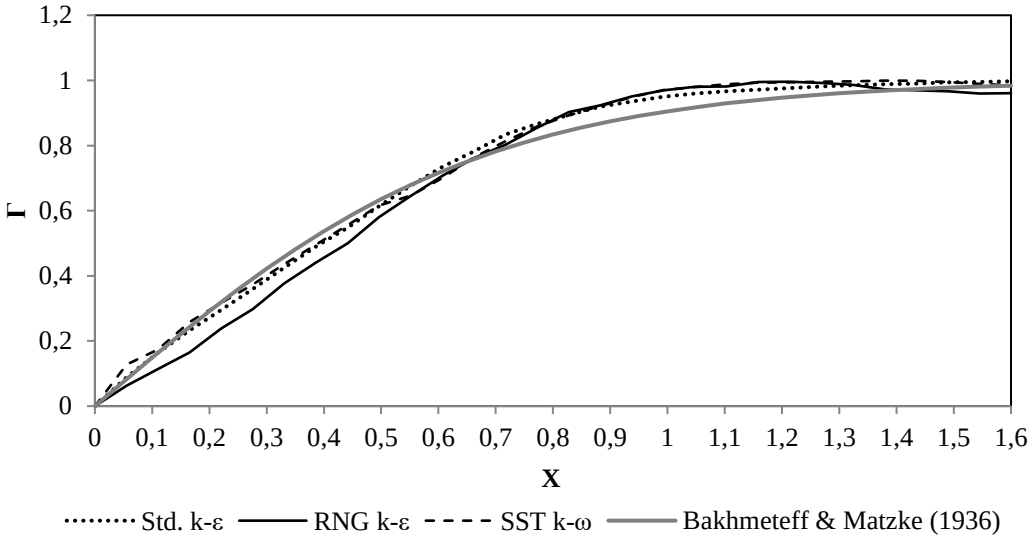

Figure 7. Water free surface level according to turbulence model used compared to previous studies.

Tab. 1 shows the accuracy of the model according to the variable predicted using the most accurate approach (RNG $k-\varepsilon$ turbulence model with $7.0mm$ size mesh). It can be deduced from such accurate results that the model proposed herein is validated and so can be applied to real-life design cases.

Variable	Model output	Reference result	Accuracy
Sequent depth (Y)	7.916	7.951	99.6%
Roller length (L_r)	$2.320m$	$2.330m$	99.6%
Hydraulic jump efficiency (η)	58.2%	59.0%	98.7%
Surface (Γ)	$-$	$-$	99.2%

Table 1. RNG $k-\varepsilon$ with $7.0mm$ mesh model outcome and analytical/experimental data comparison.

Conclusions

A three-dimensional CFD model for transient multiphase incompressible flow is developed in order to predict the behavior of classical hydraulic jumps. After analyzing the effects on the results of several model parameters, such as the mesh refinement degree, the turbulence model or the boundary conditions, a stable hydraulic jump and accurate results are obtained. The model is built using exclusively free open source code, which implies avoiding expensive software licenses. Also a problem found in other cases where OpenFOAM is used to model hydraulic jumps is addressed and solved. This problem involves the outlet boundary condition, where an additional stretch of channel with an obstacle attached to its bottom has to be added in order to force the subcritical flow to occur. Using the approach proposed in this paper, this additional stretch of channel can be removed by modifying the outlet boundary condition, with the subsequent saving of computational resources (up to 30% in some cases) with no effects on the model accuracy whatsoever.

A case study of approaching Froude number $Fr_1 = 6.125$ is simulated and the results are compared to previous studies of similar characteristics, such as that of Hager (1992) and Wu and Rajaratnam (1996). The roller length appears to be the most sensitive variable to model parameters (the SST $k-\omega$ is not even able to capture this magnitude). Some hydraulic jump variables are better reproduced in comparison with other authors' results, such as the sequent depth (error of only 0.4%), whereas others show lower accuracies, e.g. the hydraulic efficiency (error of 1.3%). The water free surface is accurately reproduced by all turbulence models in average terms, being the Standard $k-\varepsilon$ the most accurate approach. An instant observation of the results shows that the SST $k-\omega$ model surface looks more turbulent than its $k-\varepsilon$ counterparts. Anyway, the accuracy of all of the variables analyzed is above 98% in all cases so the model can be considered validated.

In the light of the results, the model is ready to be applied to real-life design cases, such as dam stilling basins, stepped spillways, river rapids, meandering channels, etc. As discussed above, the most accurate turbulence model in this kind of applications is the RNG $k-\varepsilon$, although very fine meshes are necessary to ensure good performance and this model proved to be slightly slower than the Standard $k-\varepsilon$. The latter turbulence model could be a better choice in cases where low computational requirements are preferred without compromising accuracy excessively. The Standard $k-\varepsilon$ also proved to reproduce slightly better the average water free surface.

As future work, the model is currently being used in similar applications, both theoretical, such as triangular, circular and radial hydraulic jumps, and real-life cases. Also the air entrainment and

concentration distribution in hydraulic jumps is being studied using this model and compared to experimental data.

Acknowledgements

This research was conducted thanks to the funding provided by the VALi+D R&D Program of the Generalitat Valenciana (Spain). It would not have been possible without the contribution of Daniel Valero and Beatriz Nacher of the Hydraulics Laboratory of the School of Civil Engineering (Universitat Politècnica de València).

References

1. Ahmed, F. & Rajaratnam, N. 1997 Three-dimensional turbulent boundary layers: A review. Journal of Hydraulic Research. 35, 81-98.
2. Ashgriz, N. & Poo, J. 1991 FLAIR: Flux line-segment model for advection and interface reconstruction. Journal of Computational Physics. Elsevier 93, 449-468.
3. Babb, A. & Aus, H. 1981 Measurements of air in flowing water. Journal of Hydraulic Division, ASCE. 107, 1615-1630.
4. Bakhmeteff, B. A., & Matzke, A. E. 1936 The Hydraulic Jump in Terms of Dynamic Similarity. Trans. Amer. Soc. Civ. Engrs., 100, 630-680.
5. Barton, I. 1998 Comparison of SIMPLE-and PISO-type algorithms for transient flows. International Journal for numerical methods in fluids, Wiley Online Library, 26, 459-483.
6. Belanger, J. 1841 Notes sur l'Hydraulique. Ecole Royale des Ponts et Chaussees, Paris, France.
7. Biswas, R. & Strawn, R. C. 1998 Tetrahedral and hexahedral mesh adaptation for CFD problems. Applied Numerical Mathematics, Elsevier, 26, 135-151.
8. Blazek, J. 2005 Computational Fluid Dynamics: Principles and Applications. Elsevier.
9. Blocken, B., Stathopoulos, T. & Carmeliet, J. 2007 CFD simulation of the atmospheric boundary layer: wall function problems. Atmospheric environment, Elsevier, 41, 238-252.
10. Bombardelli, F. A., Meireles, I. & Matos, J. 2011 Laboratory measurements and multi-block numerical simulations of the mean flow and turbulence in the non-aerated skimming flow region of steep stepped spillways. Environmental Fluid Mechanics. Springer 11, 263-288.

11. Borue, V., Orszag, S. & Staroslesky, I. 1995 Interaction of surface waves with turbulence: direct numerical simulations of turbulent open channel flow. Jorunal of Fluid Mechanics. 286, 1–23.
12. Bradshaw, P. 1996 Understanding and prediction of turbulent flow. International journal of heat and fluid flow. 18, 45-54.
13. Brennan, D. 2001 The numerical simulation of two phase flows in settling tanks. Imperial College of Science, Technology and Medicine (UK).
14. Bung, D. & Schlenkhoff, A. 2010 Self-Aerated Skimming Flow On Embankment Stepped Spillways-The Effect Of Additional Micro-roughness On Energy Dissipation And Oxygen Transfer. IAHR European Congress.
15. Carvalho, R. 2002 Acçoes hidrodinamicas em estruturas hidraulicas: modelacao computacional do ressalto hidraulico. Universidade de Coimbra (Portugal).
16. Casulli, V. & Cattani, E. 1994 Stability, accuracy and efficiency of a semi-implicit method for three-dimensional shallow water flow . Computers & Mathematics with Applications. 27, 99-112.
17. Caisley, M. E., Bombardelli, F. A. & Garcia, M. H. 1999 Hydraulic Model Study of a Canoe Chute for Low-head Dams in Illinois (HES 63). Hydraulic Engineering Series 63.
18. Chanson, H. 1994 Drag reduction in open channel flow by aeration and suspended load. Journal of Hydraulic Research. Taylor & Francis 32, 87-101.
19. Chanson, H. 2000 Boundary shear stress measurements in undular flows: Application to standing wave bed forms. Water Resources Research. 36, 3063-3076.
20. Chanson, H. 2013 Hydraulics of aerated flows: qui pro quo? Journal of Hydraulic Research. Taylor & Francis 51, 223-243.
21. Chau, K., Wu, C. & Li, Y. 2005 Comparison of several flood forecasting models in Yangtze River. Journal of Hydrologic Engineering, American Society of Civil Engineers, 10, 485-491.
22. Chen, W. & Chau, K. 2006 Intelligent manipulation and calibration of parameters for hydrological models. International Journal of Environment and Pollution, Inderscience, 28, 432-447.
23. Cheng, C., Chau, K., Sun, Y. & Lin, J. 2005 Long-term prediction of discharges in Manwan Reservoir using artificial neural network models. Advances in Neural Networks--ISNN 2005, Springer, 1040-1045.
24. Daly, B. J. 1969 A technique for including surface tension effects in hydrodynamic calculations. Journal of Computational Physics. Elsevier 4, 97-117.
25. De Padova, D., Mossa, M., Sibilla, S. & Torti, E. 2013 3D SPH modelling of hydraulic jump in a very large channel. Journal of Hydraulic Research, Taylor & Francis, 51, 158-173.

26. Dewals, B., André, S., Schleiss, A. & Pirotton, M. 2004 Validation of a quasi-2D model for aerated flows over stepped spillways for mild and steep slopes. Proceedings of the 6th International Conference of Hydroinformatics. 1, 63-70.
27. Farhoudi, J., Hosseini, S. & Sedghi-Asl, M. 2010 Application of neuro-fuzzy model to estimate the characteristics of local scour downstream of stilling basins. Journal of Hydroinformatics. 12, 201-211.
28. Gharangik, A. M. & Chaudhry, M. H. 1991 Numerical simulation of hydraulic jump. Journal of hydraulic engineering, American Society of Civil Engineers, 117, 1195-1211.
29. Gualtieri, C. & Chanson, H. 2007 Experimental analysis of Froude number effect on air entrainment in the hydraulic jump. Environmental Fluid Mechanics. Springer 7, 217-238.
30. Hager, W. H. 1992 Energy dissipators and hydraulic jump. Springer.
31. Hager, W. H. & Bremen, R. 1989 Classical hydraulic jump: sequent depths. Journal of Hydraulic Research. 27, 565-583.
32. Hager, W. & Sinniger, R. 1985 Flow characteristics of the hydraulic jump in a stilling basin with an abrupt bottom rise. Journal of Hydraulic Research. Taylor & Francis 23, 101-113.
33. Harlow, F. H., Welch, J. E. 1965 Numerical calculation of time-dependent viscous incompressible flow of fluid with free surface. Physics of fluids. 8, 2182.
34. Hirsch, C. 2007 Numerical computation of internal and external flows: the fundamentals of computational fluid dynamics. Butterworth-Heinemann, 1.
35. Hirt, C. & Nichols, B. 1981 Volume of fluid (VOF) method for the dynamics of free boundaries . Journal of Computational Physics . 39, 201-225.
36. Huang, H. & Prosperetti, A. 1994 Effect of grid orthogonality on the solution accuracy of the two-dimensional convection-diffusion equation. Numerical Heat Transfer, Taylor & Francis, 26, 1.20.
37. Hyman, J. M. 1984 Numerical methods for tracking interfaces. Physica D: Nonlinear Phenomena. Elsevier 12, 396-407.
38. Issa, R. I. 1985 Solution of the Implicitly Discretized Fluid Flow Equations by Operator-Splitting. Journal of Computational Physics. 62, 40-65.
39. Jang, D., Jetli, R. & Acharya, S. 1986 Comparison of the PISO, SIMPLER, and SIMPLEC algorithms for the treatment of the pressure-velocity coupling in steady flow problems. Numerical Heat Transfer, Part A: Applications, Taylor & Francis, 10, 209-228.
40. Jasak, H. 1996 Error analysis and estimation for the finite volume method with applications to fluid flows. Imperial College of Science, Technology and Medicine (UK).
41. Johnson, R. & Launder, B. 1982 Discussion of “On the calculation of turbulent heat transport downstream from an abrupt pipe expansion”. Numerical Heat Transfer, Part A Applications, Taylor & Francis, 5, 493-496.

42. Keyes, D., Ecer, A., Satofuka, N., Fox, P. & Periaux, J. 2000 Parallel Computational Fluid Dynamics ’99: Towards Teraflops, Optimization and Novel Formulations. Elsevier.
43. Kim, S.-E. & Boysan, F. 1999 Application of CFD to environmental flows. Journal of Wind Engineering and Industrial Aerodynamics, Elsevier, 81, 145-158.
44. Kucukali, S. & Chanson, H. 2008 Turbulence measurements in the bubbly flow region of hydraulic jumps. Experimental Thermal and Fluid Science, Elsevier, 33, 41-53.
45. Lafon, A. & Yee, H. 1992 On the numerical treatment of nonlinear source terms in reaction-convection equations. AIAA Materials Specialist Conference-Coating Technology for Aerospace Systems, 1.
46. Launder, B. E. & Sharma, B. I. 1974 Application of the Energy-Dissipation Model of Turbulence to the Calculation of Flow Near a Spinning Disc. Letters in Heat and Mass Transfer, 1, 131-138.
47. Liriano, S. & Day, R. 2001 Prediction of scour depth at culvert outlets using neural networks. Journal of Hydroinformatics. 3, 231-238.
48. Liu, X. & Garcia, M. H. 2008 Three-dimensional numerical model with free water surface and mesh deformation for local sediment scour. Journal of waterway, port, coastal, and ocean engineering. American Society of Civil Engineers 134, 203-217.
49. Lopez, F. & Garcia, M. H. 2001 Mean flow and turbulence structure of open-channel flow through non-emergent vegetation. Journal of Hydraulic Engineering. American Society of Civil Engineers 127, 392-402.
50. Ma, J., Oberai, A. A., Lahey Jr, R. T. & Drew, D. A. 2011 Modeling air entrainment and transport in a hydraulic jump using two-fluid RANS and DES turbulence models. Heat and Mass Transfer. Springer-Verlag 47, 911-919.
51. McDonald, P. W. 1971 The computation of transonic flow through two-dimensional gas turbine cascades. American Society of Mechanical Engineers.
52. Menter, F. R. 1993 Zonal two equation k-omega turbulence models for aerodynamic flows. AIAA paper, 2906, 1993.
53. Murzyn, F., Mouaze, D. & Chaplin, J. 2005 Optical fibre probe measurements of bubbly flow in hydraulic jumps. International Journal of Multiphase Flow. Elsevier 31, 141-154.
54. Murzyn, F. & Chanson, H. 2008 Experimental assessment of scale effects affecting two-phase flow properties in hydraulic jumps. Experiments in Fluids. Springer 45, 513-521.
55. Murzyn, F. & Chanson, H. 2009a Two-phase gas-liquid flow properties in the hydraulic jump: Review and perspectives. Nova Science Publishers .
56. Murzyn, F. & Chanson, H. 2009b Experimental investigation of bubbly flow and turbulence in hydraulic jumps. Environmental Fluid Mechanics. 2, 143–159.

57. Muttil, N. & Chau, K.-W. 2006 Neural network and genetic programming for modelling coastal algal blooms. International Journal of Environment and Pollution, Inderscience, 28, 223-238.
58. Noh, W. F. & Woodward, P. 1976 SLIC (simple line interface calculation). Proceedings of the Fifth International Conference on Numerical Methods in Fluid Dynamics June 28-July 2, 1976 Twente University, Enschede. , 330-340.
59. OpenFOAM 2011 OpenFOAM: The Open Source CFD Toolbox User Guide. The Free Software Foundation Inc.
60. Osher, S. & Sethian, J. A. 1988 Fronts propagating with curvature-dependent speed: algorithms based on Hamilton-Jacobi formulations. Journal of Computational Physics. Elsevier 79, 12-49.
61. Patankar, S. & Spalding, D. 1972 A calculation procedure for heat, mass and momentum transfer in three-dimensional parabolic flows. J. of Heat and Mass Transfer. 15, 1787-1806.
62. Peterka, A. J. 1984 Hydraulic design of stilling basins and energy dissipaters. Engineering Monograph no. 25. U.S. Bureau of Reclamation.
63. Resch, F. & Leutheusser, H. 1972 Reynolds stress measurements in hydraulic jumps. Journal of Hydraulic Research. Taylor & Francis 10, 409-430.
64. Rodrigues, M. A., Padrela, L., Geraldes, V., Santos, J., Matos, H. A. & Azevedo, E. G. 2011 Theophylline polymorphs by atomization of supercritical antisolvent induced suspensions. The Journal of Supercritical Fluids, Elsevier, 58, 303-312.
65. Romagnoli, M., Portapila, M. & Morvan, H. 2009 Computational simulation of a hydraulic jump. Mecanica Computacional. XXVIII, 1661-1672.
66. Rusche, H. 2002 Computational fluid dynamics of dispersed two-phase flows at high phase fractions. Imperial College of Science, Technology and Medicine (UK).
67. Schlichting, H. & Gersten, K. 2000 Boundary-Layer Theory. Springer.
68. Taormina, R., Chau, K.-w. & Sethi, R. 2012 Artificial neural network simulation of hourly groundwater levels in a coastal aquifer system of the Venice lagoon. Engineering Applications of Artificial Intelligence, Elsevier, 25, 1670-1676.
69. Taylor, E. S. 1959 The skewed boundary layer. Journal of Basic Engineering, Trans. ASME, Series D. 81, 297-304.
70. Thomas, S.; Hankey, W.; Faghri, A. & Swanson, T. 1990 One-dimensional analysis of the hydrodynamic and thermal characteristics of thin film flows including the hydraulic jump and rotation. Journal of heat transfer, American Society of Mechanical Engineers, 112, 728-735.
71. Toge, G. E. 2012 The significance of Froude number in vertical pipes: a CFD study. University of Stavanger, Norway.

72. Toth, E. & Brandimarte, L. 2011 Prediction of local scour depth at bridge piers under clear-water and live-bed conditions: comparison of literature formulae and artificial neural networks. Journal of Hydroinformatics. 13.
73. Ubbink, O. 1997 Numerical prediction of two fluid systems with sharp interfaces. Imperial College of Science, Technology and Medicine (UK).
74. Van Leer, B. 1982 Flux-vector splitting for the Euler equations. Eighth international conference on numerical methods in fluid dynamics, 507-512.
75. Von Karman, T. 1930 Mechanische Ahnlichkeit und Turbulenz. Nachrichten von der Gesellschaft der Wissenschaften zu Göttingen, Fachgruppe 1 (Mathematik). 5, 58-76.
76. Weller, H., Tabor, G., Jasak, H. & Fureby, C. 1998 A tensorial approach to computational continuum mechanics using object-oriented techniques. Computers in Physics. 12, 620-631.
77. Wilcox, D. 1998 Turbulence modelling for CFD. DCW Industries, La Canada, Californa (USA).
78. Witt, A., Gulliver, J. & Shen, L. 2013 Bubble visualization in a simulated hydraulic jump. The Smithsonian/NASA Astrophysics Data System.
79. Wu, S. & Rajaratnam, N. 1996 Transition from Hydraulic Jump to Open Channel Flow. Journal of Hydraulic Engineering. 122, 526-528.
80. Wu, C., Chau, K. & Li, Y. 2009 Predicting monthly streamflow using data-driven models coupled with data-preprocessing techniques. Water Resources Research, Wiley Online Library, 45.
81. Yakhot, V., Orszag, S., Thangam, S., Gatski, T. & Speziale, C. 1992 Development of turbulence models for shear flows by a double expansion technique. Physics of Fluids A: Fluid Dynamics (1989-1993), AIP Publishing, 4, 1510-1520.
82. Young, D. F., Bruce R. M., Okiishi Th. H., Huebsch, W. W. 2010 A Brief Introduction to Fluid Mechanics. John Wiley & Sons.
83. Youngs, D. L. 1984 An interface tracking method for a 3D Eulerian hydrodynamics code. Technical Rep. 44, 35-35.